Article

Not peer-reviewed version

Engineering of Extracellular Vesicles for Efficient Delivery of Prodigiosin

Ivan Guryanov *, Sirina Sabirova *, Svetlana Batasheva, Svetlana Konnova, Arthur Khannanov, Marianna Kutyreva, Ekaterina Naumenko *

Posted Date: 15 December 2025

doi: 10.20944/preprints202512.1280.v1

Keywords: prodigiosin; extracellular vesicles; drug delivery systems; prodigiosin-induced membrane vesicles; prodigiosin encapsulating

 doi:10.20944/preprints202512.1280.v1

Article

Engineering of Extracellular Vesicles for Efficient Delivery of Prodigiosin

Ivan Guryanov [1,*], Sirina Sabirova [1,*], Svetlana Batasheva [1], Svetlana Konnova [1], Arthur Khannanov [2], Marianna Kutyreva [2] and Ekaterina Naumenko [1,*]

[1] Institute of Fundamental Medicine and Biology, Kazan Federal University

[2] A.M. Butlerov Chemical Institute, Kazan Federal University

* Correspondence: ivan.guryanov@gmail.com (I.G.); sirinakurbangaleeva@gmail.com (S.S.); ekaterina.naumenko@gmail.com (E.N.)

Abstract

The therapeutic potential of prodigiosin as a hydrophobic anticancer agent can be enhanced by various approaches. One of which is the loading of PG into extracellular vesicles. Both, drug distribution and stability in aqueous media are important for targeting and accumulation, which, in turn, is important to achieve an effective drug concentration. Extracellular vesicles (EVs) are nano-sized, cell-derived vesicles with lipid bilayer membrane. EVs can be utilized as drug carriers for both water-soluble and non-water-soluble therapeutic agents. We hypothesized that EVs could effectively address the current challenges of prodigiosin delivery. Several different techniques have been developed for fabricating extracellular vesicles. These include EVs induction with cytochalasin B, prodigiosin and cultivation in serum depleted media (serum-free cultivation). Treatment with cytochalasin B has been shown to be effective for the generation of vesicles. Prodigiosin encapsulated extracellular vesicles (PG-EVs) compared to unmodified naïve ones demonstrated slightly higher charge and hydrodynamic dimensions. Which probably contributes to better stability. Overall, PG – EVs complexes might be more suitable for medical and clinical applications compared to pure forms of PG due to their cell membrane compatibility.

Keywords: prodigiosin; extracellular vesicles; drug delivery systems; prodigiosin-induced membrane vesicles; prodigiosin encapsulating

1. Introduction

Cancer is a multifactorial disease, which is why drugs for its treatment require the development of new drugs with such as multi-target inhibitors which could be a single drug with multiple inhibitory effects or combinational therapy of more than one drug so as to simultaneously hit more than one pathway all at once [1]. From this point of view, prodigiosin is a promising candidate for the development of such pharmaceutics due to its multi-target action.

Prodigiosin (PG) is a red linear tripyrrole pigment whose structural backbone consists of three pyrrole rings. It represents bioactive secondary metabolite with low molecular weight (324 Da) and molecular formula C20H25N3O [2,3]. This red pigment produced by some bacteria and other microorganisms, exhibits anti-inflammatory, anti-cancer, and antioxidant activity and can be considered as a prominent therapeutic for various diseases and conditions [1].

Many studies show that PG has immunomodulatory properties [4,5]. In depending on the type of cells and conditions of the cellular environment, PG can both stimulate and suppress the immune system, selectively acting on T and B lymphocytes, tumor-associated macrophages (TAMs) and dendritic cells (TADCs), natural killer (NK) cells, and myeloid-derived suppressor cells (MDSCs) [4,5].

Prodigiosin is involved in modulating and reprogramming the metabolism of the various immune cells in the tumor microenvironment, which, in turn, might introduce as an

 doi:10.20944/preprints202512.1280.v1

immunomodulator in cancer therapy [5]. It was found that PG can both stimulate and suppress the immune system in cell type-specific manner and depending conditions of the cellular environment. In macrophages, prodigiosin has been shown to inhibit NADPH oxidase activation by interfering with the assembly of its cytosolic components, such as p47phox and Rac [6]. Prodigiosin can have immunosuppressive effects, particularly on certain T cells [7]. PG can also reduce ROS generation induced by MC-LR (a toxin produced by cyanobacteria) by enhancing Nrf2 protein transcription factor translocation into the nucleus of HepG2 cells [8]. It has also been shown to have immunosuppressive effects and influence inflammatory processes by regulating enzymes and signaling pathways such as COX-2 and NF-κB [9]. PG, especially in the presence of copper ions, can damage DNA through oxidative mechanisms, leading to cell death. DNA damage occurs when the prodigiosin-copper complex intercalates DNA and promotes the formation of reactive oxygen species, which cleave both double-stranded DNA and RNA leading to inhibition of cell-cycle progression and cell death [10–12]. Comet assay analysis showed that PG cause a selective DNA damaged in HCT116 and Caco2 cancer cells [13]. PG could mediate macrophage activity and prostaglandin biosynthesis and may prevent the infiltration and M2 polarization of tumor-associated macrophages, which are often involved in promoting tumor growth [5].

Many studies have demonstrated a broad range of anticancer therapeutic benefits of PG. It selectively kills cancer cells through multiple mechanisms, including both caspase-dependent and independent induction of apoptosis, inhibiting Wnt/β-catenin signaling that accordingly causes cell-cycle arrest disrupting cancer cell metabolism. PG can interfere with cancer cell metabolism by regulating amino acid utilization and binding to proteins like glucose transporter 1 (GLUT1), which is involved in glucose uptake [14,15]

PG can raise the radio-sensitivity of cancer cells by inflammatory cascade induction followed by changes in redox tone (expressed by increase in SOD and GSH activities and decrease in MDA concentration), resulted in reduction of tumor growth [15]

Additionally, this drug is not excreted through ABC transporters (MDR-pumps), which are responsible for the development of chemotherapy resistance [16] so it can be used in the treatment of multiple drug-resistant cancer types.

Encapsulation has opened up opportunities for targeted drug delivery, particularly in cases where chemotherapeutic drugs have low bioavailability due to their hydrophobicity [17]. Poor water solubility of PG is a significant challenge in cancer therapy, as it can lead to poor dissolution rates and low bioavailability, requiring specialized formulation techniques to overcome these issues [1,18]. These limitations have driven extensive research into nano- and micro-encapsulation strategies, which aim to enhance its solubility, stability, and targeted delivery. It should be pointed out, research on PG encapsulation strategies is limited. The incorporation of PG into nanoparticles or nanoemulsions currently represents a key strategy to address accessibility and biocompatibility issues, thereby optimizing its therapeutic potential. Mohamed et al proposed the zein/sodium caseinate nanoparticles for encapsulation of celecoxib and prodigiosin and demonstrated good encapsulation efficiencies (EE) and bioavailability in vitro on human breast cancer MDA-MB-231 cells [19]. Nano-encapsulation with polysaccharides like β-cyclodextrin (BCD), maltodextrin (MD), gum Arabic (GA) has been shown to significantly increase its water solubility, broadening the applicability of PG in food, pharmaceutical, and cosmetic industry [20]. Anjum et al. also proposed the encapsulation of PG into nanoparticles of soy protein isolate (SPI) and demonstrated the EE up to 89% and particle size ranged from 115.63 to 181.42 nm. Peptide-guided dendrigraft poly-l-lysines nanoparticles for targeted delivery prodigiosin to choriocarcinoma was studied in vivo by Zhao et al [21]. In this study a method for targeted delivery of chemotherapeutic drugs only to cancer cells and not to normal cells in vivo using synthetic placental chondroitin sulfate-binding peptide (plCSA-BP) was investigated. Previously we demonstrated the selective cytotoxic activity of PG encapsulated in halloysite nanotubes against cancer cells, while normal cells such as HSF and MSC remained unaffected [13]. PG has also been used to graft β-cyclodextrin (CD) and chitosan (CS) magnetic nanoparticles to create an anticancer drug delivery system [22]. Fluorescence microscopy and flow

 doi:10.20944/preprints202512.1280.v1

cytometry confirm the specific effect of the nanocarriers on cancer cells. The results indicate that CS-MNPs exhibit higher activity and are better able to counteract the toxic effects of prodigiosin on cancer cells than β-CD-MNPs. Mannan-coated, enzyme-sensitive, and PG-loaded magnetic nanoparticles (PG@M-MNPs) have been used for breast and liver cancer therapy and for modeling tumor-associated macrophage immunomodulation [23]. The increased selectivity of PG@M-MNPs for cancer cells with minimal impact on normal cells has also been shown. Furthermore, the immunomodulatory activity demonstrates the potential of PG@M-MNPs to alter macrophage polarization dynamics.

Another strategy for targeted delivery of PG is the formation of microcapsules from various materials, which are designed to improve the biocompatibility, stability and bioavailability of PG. Encapsulating drugs in polymeric materials creates a platform for targeted delivery of chemotherapeutic agents. Polymer delivery systems maximize the therapeutic activity and can reduce the side effects of anticancer drugs. Dozi-Nwachukwu et al. prepared PG-loaded chitosan microspheres with high encapsulation efficiency that increased with increasing drug:polymer ratio and demonstrated a decrease in the viability of a breast cancer cell line (MDA-MB-231) [24]. Polylactic-co-glycolic acid-polycaprolactone (PLGA-PCL) microspheres have also been used to load PG for targeted delivery of anticancer drugs [25].

Another promising method for encapsulating PG may be loading it into membrane vesicles. Moreover, depending on the final drug's intended application, different cell types can be used. Extracellular vesicles (EVs) it is a general term used to describe a population of heterogeneous spherical particles ranging from 40 to 1000 nm in size, encapsulated by a double phospholipid layer [26] and released by all cell types [27]. EVs is a general term used to describe a population of heterogeneous double phospholipid layer spherical particles secreted by almost all cell types that transport proteins, lipids, nucleic acids, metabolites and membrane receptors of the cells from which they originate. There are three main groups of EVs: exosomes (30–160 nm), microvesicles (50–1000 nm), and apoptotic bodies (500–5000 nm).

EVs recognized as key mediators of intercellular communication and disease, are rapidly moving from basic research into clinical practice. Their capacity to transport bioactive molecules makes EVs a promising platform for diagnostics and targeted therapy, and interest in their clinical application is growing quickly [28]. EVs protect their cargo from degradation, which makes them important drug carriers for targeted drug delivery [29]. To date, no exosome- or extracellular-vesicle–based therapeutic has received final FDA approval, however, the roster of ongoing clinical trials provides hope for the introduction of such agents for the treatment of various diseases.

Cancer cell–derived MVs tend to interact more readily with cancer cell membranes, however, their use as drug-delivery vehicles poses safety concerns, as such MVs may promote tumor growth [30,31]. EVs from mesenchymal stem/stromal cells (MSC-EVs) can either stimulate or inhibit tumor growth in various malignancies through paracrine signaling. Some MSC-EVs have been shown to protect cancer cells from chemotherapy drugs, potentially leading to treatment failure [32], some MSC-EVs carry cargo that can suppress tumor growth by inducing apoptosis and inhibiting proliferation [33,34].

Extracellular vesicles derived from stem cells have emerged as a promising vehicle for drug delivery. EVs secreted by stem cells - including embryonic stem cells (ESCs) and MSCs - exert diverse functions, spanning embryonic development and tissue repair to cancer progression and immune modulation [28]. A recent study demonstrated that treating U266 multiple myeloma cells with MVs derived from bone marrow mesenchymal stem cells reduces their viability [35]. MSCs have been demonstrated to have immunomodulatory and regenerative functions in a variety of disease models [36]. Mesenchymal stem cells are considered an alternative treatment for rare diseases due to their immunomodulatory activity and stimulation of tissue regeneration. Their effects are driven by direct cell-mediated actions and by influences exerted through their secretome - the set of molecules and exosomes released into the medium [37]. MSC-EVs are small, cross the blood–brain barrier, and exhibit low immunogenicity with high biocompatibility [38]. In preclinical models, MSC-derived

 doi:10.20944/preprints202512.1280.v1

exosomes enhanced wound healing, promoted bone regeneration, and facilitated cartilage repair by modulating inflammation, angiogenesis, cell proliferation, and matrix synthesis [39]. Beyond MSCs, common sources of EVs include tumor cells, human embryonic kidney 293 (HEK293) cells, and dendritic cells (DCs). HEK293 cells are favored due to their high transfection efficiency, rapid growth, and ease of culture. HEK293 cells produce large quantities of exosomes, making them an ideal model for obtaining drug-loaded exosomes.

There are no reports yet on attempts to load PG into CF, so in our study, we first formed MVs as a prototype of an EV-based drug delivery system, loaded MVs with PG, and performed a comparative analysis of the size, charge, and prodigiosin content in MV induced by cytochalasin B and PG.

2. Materials and Methods

2.1. Cells and Culture Conditions

Mesenchymal stem cells (MSCs) were isolated from rat adipose tissue by digestion using 0.2% collagenase from crab hepatopancreas (Biolot, St. Petersburg, Russia), according to the previously developed protocol [40].

The cell lines HEK 293 (Human Embryonic Kidney 293 was isolated from the kidney of a human embryo, ATCC # CRL-1573), were obtained from the American Type Culture Collection (ATCC, Manassas, VA, USA). Cells were cultured using two different types of cell culture media, α-MEM (Alpha-Minimum Essential Medium) and DMEM/F12 (Dulbecco's Modified Eagle Medium/Nutrient Mixture F-12) (PanEco, Moscow, Russia) with 10% FBS (HyClone, Logan, UT, USA), 2 mM of L-glutamine and antibiotics penicillin (100 U/mL), and streptomycin (100 μg/mL) (PanEco, Moscow, Russia). Cells were incubated at 37 °C and 5% CO2 and maintained according to the standard protocols. Cell morphology was examined by an Axio Observer.Z1 (CarlZeiss, Jena, Germany) microscope and Axio Vision Rel. 4.8 software.

2.2. Isolation of Prodigiosin and Cytochalasin B-Induced Membrane Vesicles

Vesicles were isolated from MSCs (MSC CBiMVs) and HEK 293 cells (HEK CBiMVs) using cytochalasin B (cytochalasin B from Drechslera dematioidea, #C6762-5MG, Sigma-Aldrich, St. Louis, MO, USA) as previously described [41]. When the cell culture reached 85-90% confluency, the medium was removed, culture was washed twice with PBS and the cells were detached with 0.25% trypsin-EDTA solution (PanEco, Moscow, Russia). Then the cells were washed with PBS, centrifuged, resuspended and incubated in modified serum-free DMEM (4×106 cells in 2ml) containing 10 μg/mL cytochalasin B (Sigma-Aldrich, St. Louis, MO, USA) or prodigiosin (50 ng/ml and 250 ng/ml) for 30 min at 37 °C in a humidified atmosphere with 5% CO2. During incubation cells were vortexed twice: after 15 min incubation (for 30s) and for 60s after incubation. Next, a series of subsequent centrifugations were carried out: 700 rpm for 10 min (supernatant was collected), 1400 rpm for 10 min (supernatant was collected) 12,000 rpm for 15 min (supernatant was discarded). After resuspending the pellets, the MV suspension was passed through 5 μm syringe filter.

2.3. Loading of MVs with Prodigiosin

The samples obtained in previous step were divided into two type of probes - for additional loading with prodigiosin/sonification and without it, half of which were added 250 ng of prodigiosin. A mixture of MVs with PG (250 ng) was sonicated using an ultrasonic homogenizer Bandelin SONOPULS HD 2200, 70 Вт with booster horn SH 213 G, tip TT13 (BANDELIN electronic GmbH & Co. KG, Berlin, Germany) with an amplitude of 45% for 6 cycles, each cycle included 6 on/off periods of 30 s with a cooling period of 2 min between each cycle [42].

After resuspending the precipitates, the MV suspension was passed through filter (5 μm). The precipitate containing CBiMVs was washed with PBS. After centrifugation, the supernatant was

 doi:10.20944/preprints202512.1280.v1

removed, and the resulting CBiMV pellet was dissolved in the culture medium, PBS, or another buffer, depending on the purpose of further experiments.

2.4. Protein Concentration Measurement

The CBiMVs and PGiMVs were incubated in lysing solution (50 mM Tris-HCl pH 7.4, 1% NP 40, 0.5% sodium deoxychalate, 0.1% SDS, 150 mM NaCl, 2 mM EDTA, and 1 mM PMSF) for 30 min on ice. Then, the resulting mixture was centrifuged at 14,000 rpm for 15 min at 4 °C. Total protein concentration was determined in supernatant using the Pierce™ BCA Protein Assay Kit (ThermoScientific, Waltham, MA, USA) according to the manufacturer's instructions.

2.5. Hydrodynamic Diameters and Zeta-Potential Analysis

Aqueous hydrodynamic diameters and zeta-potential of EVs were measured in water at 25 °C using a Malvern Zetasizer Nano ZS instrument and standard plastic cells.

2.6. Microscopy

Suspensions of EVs and CBiMVs were gradually treated with ethanol solutions with 10-96% to dehydrate them, resulting suspensions were dropped onto clean glass cover slips in 24 well plate and centrifuge at 3000 rpm for 30 min. Then, EVs were fixed with 10% formalin for 15 min, washed twice with ultra-pure water, dehydrated with an ethanol gradient from 30% to absolute and air-dried for 24 h. Visualization was performed on an Auriga field-emission scanning electron microscope (Carl Zeiss) using an Inlens secondary electron detector at an accelerating voltage of 5 keV and an electron beam current of 300 pA. Prior to the study, the samples were sputter-coated with gold to ensure electron conductivity; the sputtering thickness was ~10 nm

Enhanced dark field (EDF) microscopy images were obtained using an Olympus BX51 upright microscope equipped with a CytoViva® enhanced dark-field condenser and a DAGE CCD camera.

2.7. Flow Cytometry Analysis

The pellets obtained after EVs and CBiMVs isolation were analyzed using flow cytometry. A mixture of calibration particles of 0.22, 0.45, 0.88, 1.34, and 3.4 μm (Cat. No. PPS-6K, Spherotech, Lake Forest, IL, USA) was used for the calibration of the CytoFLEX S (Beckman Coulter, Brea, CA, USA). Analysis of the yield of EVs and CIMVs after a series of centrifugations at 2300 g for 25 min, 10,000 g for 45 min, and 100,000 g for 90 min was performed using a CytoFLEX S (Beckman Coulter, USA) flow cytometer. Each sample was recorded within 60 s.

2.8. Nanoparticle Tracking Analysis (NTA)

The colloidal properties were studied by the NTA method on a NanoSight LM—10 instrument (Malvern Panalytical, Malvern, UK). CMOS cameras C11440-50B with an FL-280 Hamamatsu Photonics (Shizuoka, Japan) image capture sensor were used as a detector. Measurements were taken in a special cuvette for aqueous solutions, equipped with a 405 nm laser (version CD, S/N 2990491) and a sealing ring made of Kalrez material. The temperature was taken with an OMEGA HH804 contact thermometer (Engineering, Inc., Stamford, CT, USA) for all measurements. Samples for analysis were detected and injected into the measuring cell with a 1 mL glass 2-piece syringe (tuberculin) through the Luer (Hamilton Company, Reno, NV, USA). To increase the statistical dose, the sample was pumped through the measuring chamber by using a piezoelectric dispenser. Each sample was detected sequentially six times; the recording time was sequential and amounted to 60 s. For processing the footage of the Nanosight instrument, NTA 2.3 software applications (build 0033) and OriginPro program package were used; the Gaussian function was used throughout, as described previously [43–46].

2.9. Statistical Analysis

 doi:10.20944/preprints202512.1280.v1

Statistical analysis was performed using Student's *t*-test (GraphPad Software, San Diego, CA, USA) with a significance level of $p < 0.05$..

3. Results

3.1. Quantitative Characterization of Microvesicles

MVs' protein content was measured using Quantitative BCA Protein Assay and Nanoparticle tracking analysis (NTA) was used to quantify colloidal properties including the number of MVs in a sample volume and their size distribution. Quantitative analysis of MVs protein content showed that there were no significant differences in the number of MVs induced from HEK293 and MSC cells induced by cytochalasin B and PG (Figure 1A).

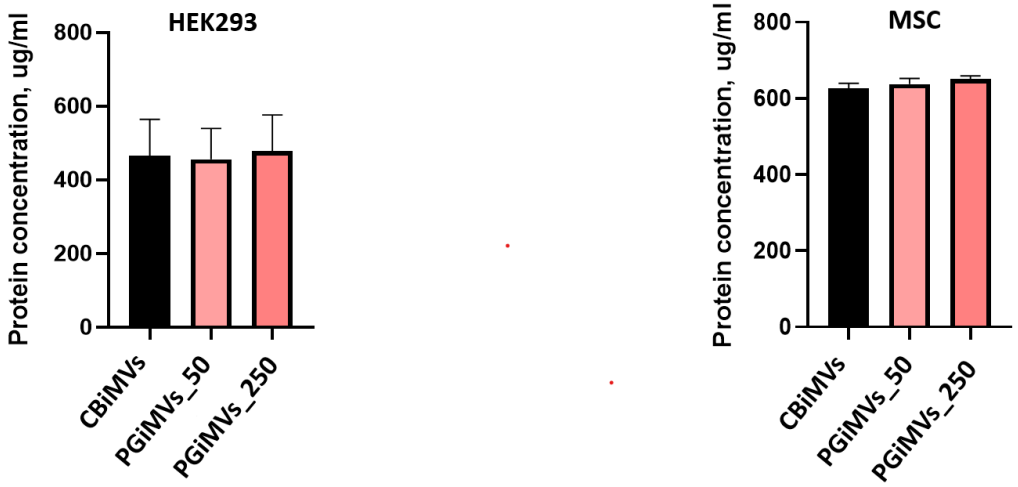

Samples	HEK293		MSCs	
	Dh (nm)	Particles ($\times 10^8$/ml)	Dh (nm)	Particles ($\times 10^8$/ml)
CBiMVs	196±7.3	6.21±0.19	187±9.0	15.6±0.6
PGiMVs_50	185±12.0	6.60±0.18	202±9.0	14.6±0.5
PGiMVs_250	101±15.0	2.38±0.80	142±3.0	7.2±0.5
CBiMVs+250US	87±17.0	0.77±0.03	125±6.0	6.3±0.4
PGiMVs_50+250US	47±20.0	0.54±0.06	222±5.0	15.2±0.4
PGiMVs_250+250US	60±13.0	0.93±0.23	147±6.0	6.7±0.3

Figure 1. Protein concentration measurement (A) and determination of the size and concentration of MVs in NTA analysis (B): recording time was sequential and amounted to 60 s, laser—405 nm; camera level—10; detection threshold—7; slider shutter—1206; camera Shutter (ms) - 8.75 ms, slider gain—245; syringe pump speed—50; each sample was detected sequentially six times.

As can be seen from the particle size distribution (Dh) graph in the table (Figure1B, samples CBiMVs+250US, PGiMVs_50+250US and PGiMVs_250+250US), ultrasound can provoke the disruption of membrane integrity of the cytochalasin B and PG induced MVs (CBiMVs and PGiMVs). Then they self-assemble into more stable, smaller aggregates in case of HEK293 cells. Moreover, a significant decrease in the overall particle concentration indicates that some vesicle components remain as individual molecules in solution. Characteristically, vesicles derived from MSCs are more resistant to external physical stimulation, which is generally preferable for targeted delivery systems.

 doi:10.20944/preprints202512.1280.v1

3.2. Hydrodynamic Diameters (Dh) and Zeta Potentials (ζ) of MVs Analysis

The typical characteristics of EVs including exosomes and MVs are their size and shape, as these parameters can affect other properties such as colloidal stability [47]. To characterize particle size and charge of different types of MVs developed in our study, the hydrodynamic diameters (Dh) and zeta potentials (ζ) of MVs were determined by dynamic light scattering (DLS) and laser Doppler velocimetry (Figure 2). We suggested that PG as a cargo and inducer of MVs production as well as method of loading can influence the surface plasmon resonance oscillations and change the size, surface charge, and stability of the synthesized MVs.

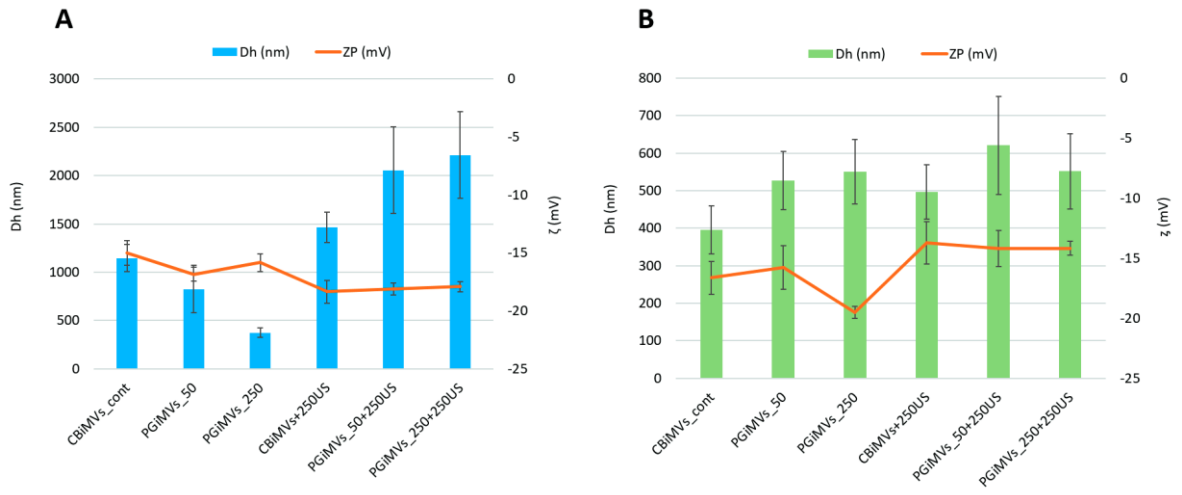

Figure 2. Hydrodynamic diameters (Dh, nm) and zeta potentials (ζ, mV) of MVs obtained by induction with cytochalasin B (CBiMVs) and prodigiosin (PGiMVs) from HEK293 (A) and rat MSC (B).

As evidenced by the values of the zeta potential in Figure 2, the charge of MVs induced from MSCs (-13.73 to -19.5) and HEK293 cells (-15.02 to -18.35) ranges from -13 mV to -20 mV. This value significantly increases after ultrasound treatment with the addition of PG for HEK microvesicles, while it decreases slightly for MSC vesicles. Zeta potential for HEK 293 derived Cytochalasin B induced MVs (CBiMVs) was -15.02 mV at a hydrodynamic diameter 1147 nm. After addition of 250ng PG and US treatment, the size of the MV increased by 27%, reaching a value of 1463 nm, the zeta potential of CBiMV+250 was -18.35mV. This value of zeta potential indicates good colloidal stability of microvesicles.

The sizes of PG-induced vesicles from HEK293 cells varied significantly. At 50 ng of PG, the vesicle sizes were similar to those of CBiMVs, reaching a value of 826 nm and a zeta potential of -16.83 mV. The smallest microvesicles from HEK293 cells were induced using 250 ng of PG (Dh – 373 nm, ζ -15.83 mV). Loading of PG and US of PG-induced microvesicles resulted in their increase by more than 2 folds in PGiMVs_50+250, Dh - 2056 nm (ζ -18.11 mV) and PGiMVs_250+250, Dh – 2211 nm (ζ -17.91 mV). In comparison to HEK293 derived CBiMVs, CBiMVs from MSCs had significantly lower (Dh) hydrodynamic diameter (on average about 396 nm) and slightly higher zeta potential values of -16.63 mV. Fivefold increase in the amount of PG for MV induction leads to a slight increase in the size of 551 nm PGiMVs_250 versus 527 nm PGiMVs_50 and an increase in the zeta potential from -15.76 mV to -19.5 mV. Figure 2 shows that after ultrasonic loading of the drug into PG-induced MVs from MSCs the charge decreases from −15.76 mV (PGiMVs_50) to −14.2 mV (PGiMVs_50+250US) and from −19.76 mV (PGiMVs_250) to −14.16 mV (PGiMVs_250+250US). Moreover, the Dh changed only in PGiMVs_50 to 621 nm. Overall, PG induced and PG-loaded MVs from MSCs were significantly smaller and less polydisperse in size.

The increase in the polydispersity index, which can reflect a wide range of indicators, is possibly the result of an increase in the number of aggregates from a multitude of MVs. This view is supported by CytoViva enhanced darkfield hyperspectral images (Figure 3). Aggregation became more

 doi:10.20944/preprints202512.1280.v1

intensive upon the addition of PG to the MVs suspension, as well as the partial release of PG from the MVs during ultrasonic treatment. The highest polydispersity index (close to 1), is demonstrated by samples PGiMVs_50+250US and PGiMVs_250+250US.

Thus, CBiMVs+250US from HEK293FT and PGiMVs250 from rMSCs possess best electrostatic stability due to the strong repulsive force between the charged particles.

3.3. Visualisation of MVs

Dark-field photographs of different samples of MVs demonstrate the abundance and shape of MVs (Figure 3). Dark-field microscopy with hyperspectral analysis demonstrated different reflectance spectra for control and PG-loaded microvesicles (Figure S2). The reflectance spectrum of control vesicles was lower in intensity than that of PG-loaded microvesicles and showed a gradual decrease from 440-460 nm to 1000 nm. The reflectance spectrum of PG-loaded microvesicles demonstrated a prominent peak around 565 nm, the position of which was very close to that of the known PG fluorescence emission peak at about 560 nm [Tenconi et al., 2013; Brehl et al., 2022]. Thus, hyperspectral analysis additionally confirmed the presence of PG in PG-loaded microvesicles.

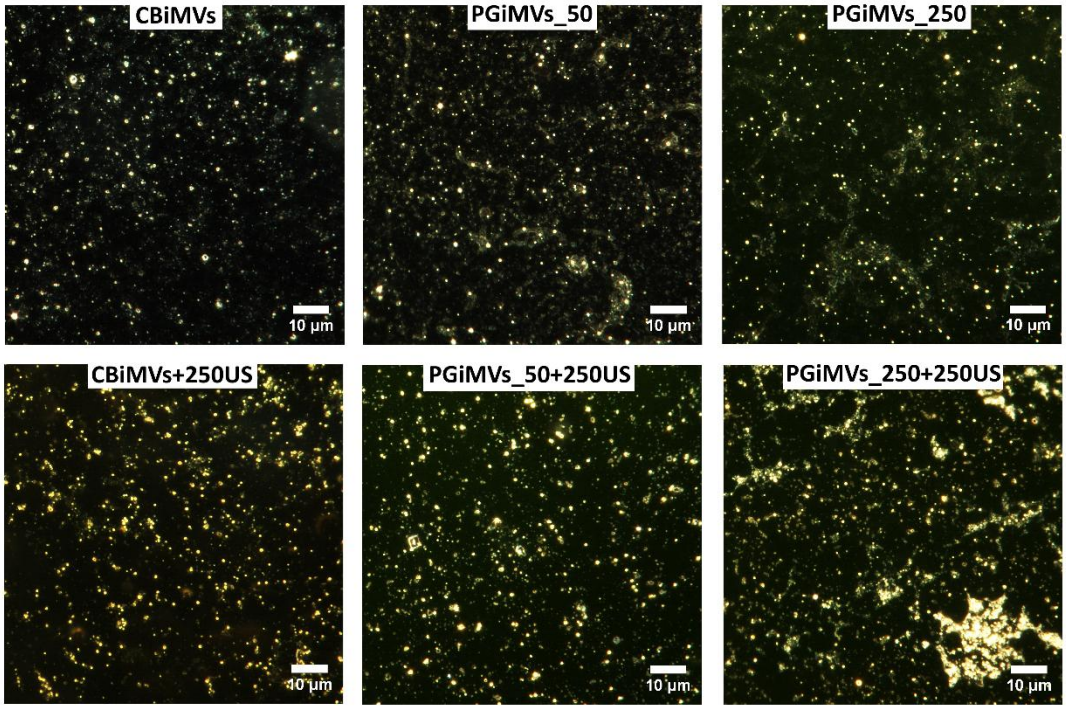

Figure 3. CytoViva enhanced darkfield hyperspectral images (100×) of MVs induced by Cytochalasin-B or prodigiosin from HEK 293FT cells.

SEM image represents the topography of the MVs surface, which is obtained by scanning it with a focused electron beam and detecting secondary electrons emitted by the atoms in the analysed area. SEM allowed to visualize the morphology of individual MVs obtained after induction by PG and cytochalasin B with and without US treatment (Figure 4). Agglomeration occurred due to the drying process before the SEM analysis.

 doi:10.20944/preprints202512.1280.v1

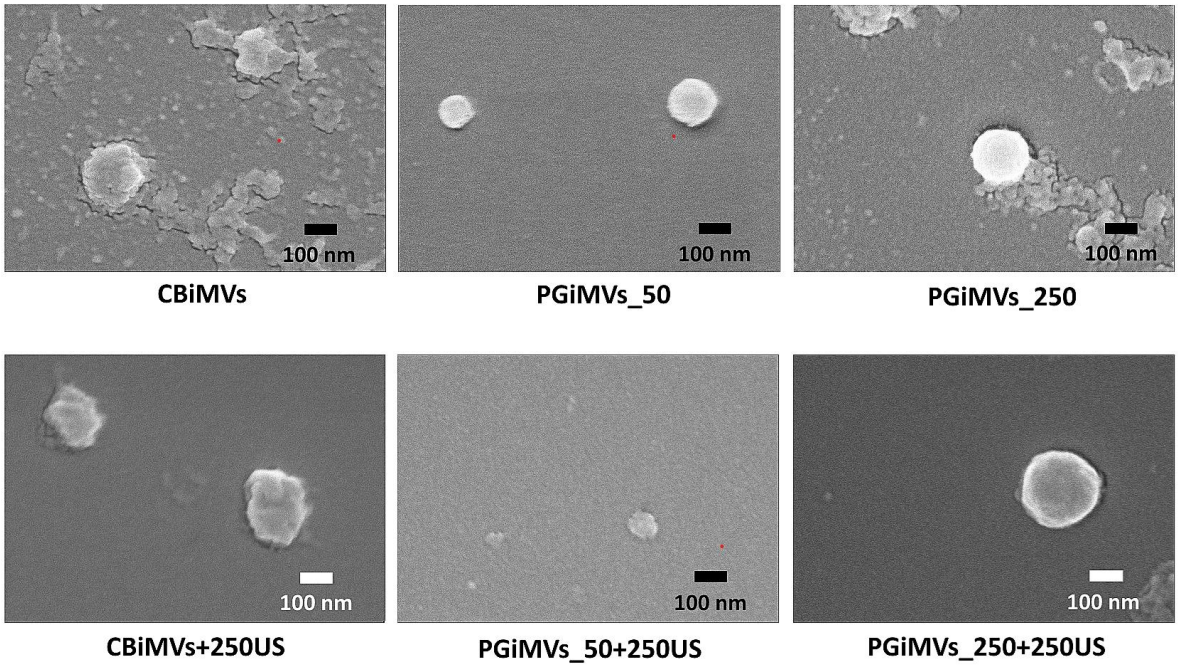

Figure 4. Scanning electron microscopy (SEM) images of Cytohalasin-B and Prodigiosin induced microvesicles from MSC.

3.4. Flow Cytometry Analysis

Different populations of MVs in flow cytometry are distinguished by their varied sizes, morphologies, and surface PG contents substances. Flow cytometry analysis showed that the gMFI of PG in HEK293FT-derived microvesicles did not differ significantly between vesicles before and after additional loading with 250 μM PG for any induction method (paired two-tailed t-test, n = 3 independent experiments: CBiMVs vs CBiMVs+250US, p = 0.40; PGiMVs_50 vs PGiMVs_50+250US, p = 0.80; PGiMVs_250 vs PGiMVs_250+250US, p = 0.86). For MSCs-derived microvesicles, only two independent experiments were performed (n = 2). Additional loading with 250 μM PG tended to increase fluorescence of CBiMVs approximately three-fold and to decrease fluorescence of PGiMVs_50 approximately 6-7-fold in both experiments, whereas the effect on PGiMVs_250 was inconsistent between experiments. Due to the very small sample size (n = 2), these observations are descriptive and did not reach statistical significance in paired two-tailed t-tests.

Different populations of microvesicles (MVs) in flow cytometry are distinguished by their varied sizes, morphologies, and surface prodigiosin contents substances. Flow cytometry analysis showed that the gMFI of PG in HEK293FT-derived microvesicles did not differ significantly between vesicles before and after additional loading with 250 μM PG for any induction method (paired two-tailed t-test, n = 3 independent experiments: CBiMVs vs CBiMVs+250US, p = 0.40; PGiMVs_50 vs PGiMVs_50+250US, p = 0.80; PGiMVs_250 vs PGiMVs_250+250US, p = 0.86). For MSCs-derived microvesicles, only two independent experiments were performed (n = 2). Additional loading with 250 μM PG tended to increase fluorescence of CBiMVs approximately three-fold and to decrease fluorescence of PGiMVs_50 approximately 6-7-fold in both experiments, whereas the effect on PGiMVs_250 was inconsistent between experiments. Due to the very small sample size (n = 2), these observations are descriptive and did not reach statistical significance in paired two-tailed t-tests.

Overlaid histograms show prodigiosin-PE signal in CBiMVs and CBiMVs+250US, PGiMVs_50 and PGiMVs_50+250US, and PGiMVs_250 and PGiMVs_250+250US. Each row (R1–R2) represents an independent experiment. The vertical marker indicates the gate used to define prodigiosin-positive (PG^+) microvesicles; the corresponding percentage of PG^+ events is shown on each plot. In both cell types, the proportion of PG^+ vesicles remains very low under most conditions and varies significantly

 doi:10.20944/preprints202512.1280.v1

between replicates. For PGiMVs_50 and PGiMVs_250, the additional load of PG does not significantly increase the proportion of PG^+ microvesicles: the histograms for the two conditions almost completely overlap, and the PG^+ percentages are close to zero. Collectively with quantitative analysis (gMFI), these data indicate that under the induction and loading conditions used, the efficiency of PG accumulation in vesicles remains low and highly variable. The different amount of PG in microvesicles from different cells is primarily due to different cellular uptake of PG

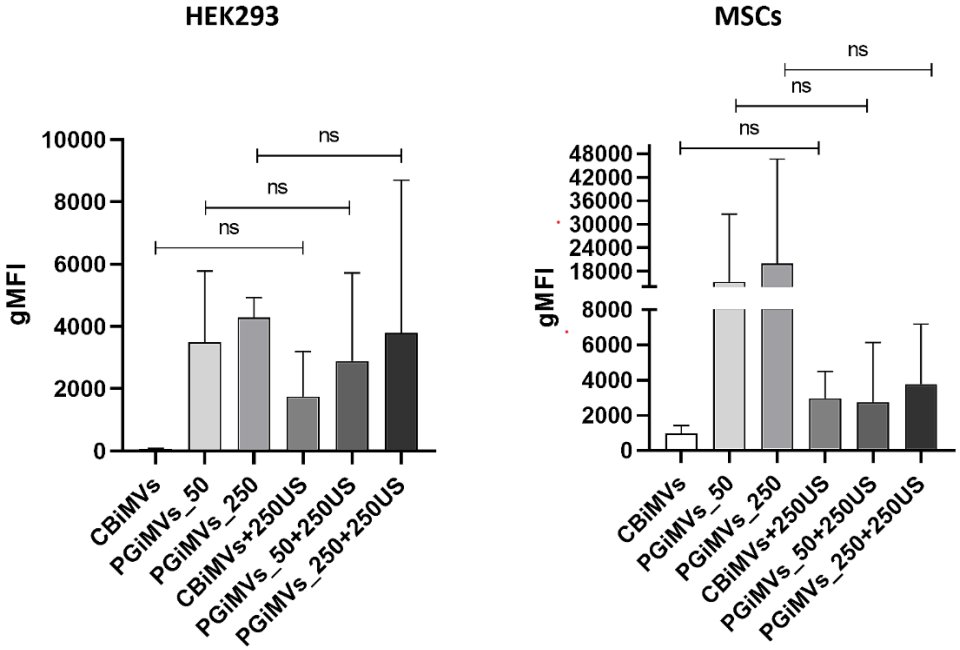

Figure 5. Flow cytometry (FCM) analysis of a Cytochalasin B and prodigiosin induced microvesicles from HEK293 and MSC cells. Upper – MVs from HEK293, lower – MVs from MSCs.

4. Discussion

Packaging therapeutic agents into membrane vesicles offers several advantages over other delivery systems, but the most important is the increased bioavailability of the administered compounds due to the affinity of microvesicles for cell membranes. Membrane vesicles can fuse with the cell membrane, combining their lipid layers and releasing their contents into the cell [48].

The vesicles are equipped with specific proteins (in particular, SNARE proteins) that recognize and bind to corresponding proteins on the cell membrane. Upon contact, the lipid layers mix and pores form, allowing the contents to enter the cell. SNAREs form an extremely stable complex, allowing membrane tethering and subsequent MV fusion with the plasma membrane [49]. An advantage of microvesicles as a delivery system is the high efficiency of delivery of lipophilic compounds [50].

Despite the advantages of high drug loading efficiency and continuous drug release, sonication may have adverse effects on the structure of exosomes, causing changes in the spherical shape and hydrophobic drug loading efficiency, as well as inducing exosome aggregation. Nevertheless, sonication remains a popular method for developing novel exosomal drug delivery systems due to its great potential for optimizing drug delivery [51].

As a result, in many cases, the sonication method provides higher loading efficiency than co-incubation and electroporation. In a study on the introduction of paclitaxel into macrophage-derived exosomes, the throughput of sonication reached 28.3%, whereas alternative methods such as incubation and electroporation yielded throughputs of only 1.4% and 5.3%, respectively [52].

Similarly, in a study investigating gemcitabine loading, sonicated exosomes demonstrated higher loading efficiency (11.7 ± 3.7%) than incubated exosomes alone (2.8 ± 0.7%) [53]. In our study,

 doi:10.20944/preprints202512.1280.v1

we also observed an increase in the level of loaded prodigiosin when using ultrasonic treatment; however, the disadvantages of this method, leading to particle aggregation, do not allow us to consider this method optimal for loading prodigiosin.

Extracellular vesicles (EVs) are characterized in terms of physical properties, such as particle size, concentration, surface charge, density, and biological properties, i.e., their internal and external biomolecular composition, such as membrane-associated antigens [54], techniques such as electron microscopy [55], atomic force microscopy [56], dynamic light scattering (DLS), flow cytometry [57], and nanoparticle tracking analysis (NTA) [58] can be used to measure the size, shape, and density of EV particles.

To analyze the size and amount of MVs obtained in our study we used NTA which has become the gold standard for characterizing the physical properties of microvesicles (MVs) and other extracellular vesicles. Generally, NTA is well suited to study exosomes [59]. This method provides a unique opportunity to rapidly analyze the size, concentration, and distribution of nanoparticles in suspension, which is critical for their study as biomarkers and functional agents. NTA is the first and essential method for analyzing MVs after isolation. It allows for the determination of the particle size profile (the peak for MVs is typically in the 100-500 nm range) and the precise particle concentration. This is essential for standardizing experiments and comparing the efficiency of different isolation protocols (e.g., ultracentrifugation vs. chromatography) [60,61]. When studying the mechanisms of MV formation or their effects on target cells, it is necessary to accurately dose the amount of vesicles added to the experiment. NTA allows for the addition of a precise number of particles to the cell culture rather than an arbitrary volume of the sample, significantly improving the reproducibility of the results. So NTA in this study allowed to evaluate particle size distribution and stability depending on the conditions of MVs formation. These data were also supported by the protein concentration data, and taken together, NTA and protein concentration analysis allowed us to determine the concentration of microvesicles in solution.

Examining the electrical properties of small EVs, particularly their surface charge distribution, could contribute to the development of essential new technologies in the rapidly expanding field of EV research [62,63]. Zeta potential (ZP) is a widely used approach for assessing the surface potential of EVs, serving as an indicator of surface charge and colloidal stability, which are affected by surface chemistry, bioconjugation, and the specific theoretical model employed [47]. The surface of microvesicles has a negative charge, which is due to the presence of phospholipids with negatively charged groups on the outer side of the membrane, such as phosphatidylserine [47,64]. Prodigiosin possesses a specific charge and hydrophobicity that can influence the surface charge of vesicles, altering their zeta potential. It contains three pyrrole rings and one propionic group, but its underlying charge is not fixed but rather pH-dependent.

The polydispersity index (PDI) is a metric measured by a Zetasizer instrument used to characterize the particle size distribution of a sample. A low PDI value indicates a narrow, uniform size distribution, while a high PDI value indicates a broad, non-uniform distribution. Zetasizer instruments, manufactured by companies such as Malvern Panalytical, use techniques such as dynamic light scattering to measure PDI, which is critical for applications in pharmaceuticals, paints, inks, and other industries [65]. Nanoparticles with a zeta potential between -10 and +10 mV are considered approximately neutral [66]. While nanoparticles with zeta potentials of greater than +30 mV or less than -30 mV are considered strongly cationic and strongly anionic, respectively.

Author Contributions: Conceptualization, I.G., E.N. and S.S.; methodology, I.G., S.S.; validation, I.G., S.S. and E.N.; formal analysis, I.G.; investigation, S.S., A.K., S.B. and S.K.; writing—original draft preparation, I.G., S.S., E.N., A.K. and S.B.; writing—review and editing, I.G.; visualization, S.K., S.B.; supervision, I.G.; project administration, I.G. All authors have read and agreed to the published version of the manuscript.

Funding: The research was supported by the Russian Science Foundation (RSF) under grant No. 25-25-00011.

Data Availability Statement: all data presented in the study.

 doi:10.20944/preprints202512.1280.v1

Conflicts of Interest: The authors declare no conflict of interest.

References

1. Guryanov, I.; Naumenko, E. Bacterial Pigment Prodigiosin as Multifaceted Compound for Medical and Industrial Application. Appl. Microbiol. 2024, 4, 1702–1728, doi:10.3390/applmicrobiol4040115.
2. Song, M.-J.; Bae, J.; Lee, D.-S.; Kim, C.-H.; Kim, J.-S.; Kim, S.-W.; Hong, S.-I. Purification and Characterization of Prodigiosin Produced by Integrated Bioreactor from Serratia Sp. KH-95. J. Biosci. Bioeng. 2006, 101, 157–161, doi:10.1263/jbb.101.157.
3. Guryanov, I. D., Karamova, N. S., Yusupova, D. V., Gnezdilov, O. I., & Koshkarova, L. A. The bacterial pigment prodigiosin and its genotoxic properties. Bioorganic Chemistry. 2013, 39, 121–128, doi:10.7868/S0132342312060048.
4. Nie, H.; Li, Y.; Lu, X.-L.; Yan, J.; Liu, X.-R.; Yin, Q. Prodigiosin Derived from Chromium-Resistant Serratia Sp. Prevents Inflammation and Modulates Gut Microbiota Homeostasis in DSS-Induced Colitis Mice. Int. Immunopharmacol. 2023, 116, 109800, doi:10.1016/j.intimp.2023.109800.
5. Anwar, M.M.; Albanese, C.; Hamdy, N.M.; Sultan, A.S. Rise of the Natural Red Pigment 'Prodigiosin' as an Immunomodulator in Cancer. Cancer Cell Int. 2022, 22, 419, doi:10.1186/s12935-022-02815-4.
6. Nakashima, T.; Iwashita, T.; Fujita, T.; Sato, E.; Niwano, Y.; Kohno, M.; Kuwahara, S.; Harada, N.; Takeshita, S.; Oda, T. A Prodigiosin Analogue Inactivates NADPH Oxidase in Macrophage Cells by Inhibiting Assembly of P47phox and Rac. J. Biochem. 2007, 143, 107–115, doi:10.1093/jb/mvm196.
7. Han, S.B.; Kim, H.M.; Kim, Y.H.; Lee, C.W.; Jang, E.-S.; Son, K.H.; Kim, S.U.; Kim, Y.K. T-Cell Specific Immunosuppression by Prodigiosin Isolated from Serratia Marcescens. Int. J. Immunopharmacol. 1998, 20, 1–13, doi:10.1016/S0192-0561(97)00062-3.
8. Chen, J.; Li, Y.; Liu, F.; Hou, D.-X.; Xu, J.; Zhao, X.; Yang, F.; Feng, X. Prodigiosin Promotes Nrf2 Activation to Inhibit Oxidative Stress Induced by Microcystin-LR in HepG2 Cells. Toxins (Basel). 2019, 11, 403, doi:10.3390/toxins11070403.
9. Lin, S.-R.; Chen, Y.-H.; Tseng, F.-J.; Weng, C.-F. The Production and Bioactivity of Prodigiosin: Quo Vadis? Drug Discov. Today 2020, 25, 828–836, doi:10.1016/j.drudis.2020.03.017.
10. Kimyon, Ö.; Das, T.; Ibugo, A.I.; Kutty, S.K.; Ho, K.K.; Tebben, J.; Kumar, N.; Manefield, M. Serratia Secondary Metabolite Prodigiosin Inhibits Pseudomonas Aeruginosa Biofilm Development by Producing Reactive Oxygen Species That Damage Biological Molecules. Front. Microbiol. 2016, 7, doi:10.3389/fmicb.2016.00972.
11. Melvin, M.S.; Tomlinson, J.T.; Saluta, G.R.; Kucera, G.L.; Lindquist, N.; Manderville, R.A. Double-Strand DNA Cleavage by Copper·Prodigiosin. J. Am. Chem. Soc. 2000, 122, 6333–6334, doi:10.1021/ja0000798.
12. Lins, J.C.L.; Melo, M.E.B.D.E.; do Nascimento, S.C.; Adam, M.L. Differential Genomic Damage in Different Tumor Lines Induced by Prodigiosin. Anticancer Res. 2015, 35 6, 3325–3332.
13. Guryanov, I.; Naumenko, E.; Akhatova, F.; Lazzara, G.; Cavallaro, G.; Nigamatzyanova, L.; Fakhrullin, R. Selective Cytotoxic Activity of Prodigiosin@halloysite Nanoformulation. Front. Bioeng. Biotechnol. 2020, 8, doi:10.3389/fbioe.2020.00424.
14. Yang, H.-A.; Han, T.-H.; Haam, K.; Lee, K.-S.; Kim, J.; Han, T.-S.; Lee, M.-S.; Ban, H.S. Prodigiosin Regulates Cancer Metabolism through Interaction with GLUT1. Nat. Prod. Res. 2025, 39, 5264–5271, doi:10.1080/14786419.2024.2367241.
15. ElBakary, N.M.; Anees, L.M.; Said Shahat, A.; Mesalam, N.M. A Promising Natural Red Pigment "Prodigiosin" Sensitizes Colon Cancer Cells to Ionizing Radiation, Induces Apoptosis, and Impedes MAPK/TNF-α/NLRP3 Signaling Pathway. Integr. Cancer Ther. 2025, 24, doi:10.1177/15347354251342764.
16. Llagostera, E.; Soto-Cerrato, V.; Joshi, R.; Montaner, B.; Gimenez-Bonaf??, P.; P??rez-Tom??s, R. High Cytotoxic Sensitivity of the Human Small Cell Lung Doxorubicin-Resistant Carcinoma (GLC4/ADR) Cell Line to Prodigiosin through Apoptosis Activation. Anticancer. Drugs 2005, 16, 393–399, doi:10.1097/00001813-200504000-00005.
17. Naumenko, E.; Guryanov, I.; Gomzikova, M. Drug Delivery Nano-Platforms for Advanced Cancer Therapy. Sci. Pharm. 2024, 92, 28, doi:10.3390/scipharm92020028.

 doi:10.20944/preprints202512.1280.v1

18. Rashidi, M.; Jebali, A. Liposomal Prodigiosin and Plasmid Encoding Serial GCA Nucleotides Reduce Inflammation in Microglial and Astrocyte Cells by ATM/ATR Signaling. J. Neuroimmunol. 2019, 326, 75–78, doi:10.1016/j.jneuroim.2018.11.014.
19. Mohamed, W.A.; El-Nekhily, N.A.; Mahmoud, H.E.; Hussein, A.A.; Sabra, S.A. Prodigiosin/Celecoxib-Loaded into Zein/Sodium Caseinate Nanoparticles as a Potential Therapy for Triple Negative Breast Cancer. Sci. Rep. 2024, 14, 181, doi:10.1038/s41598-023-50531-4.
20. Anjum, N.; Wani, S.M.; Padder, S.A.; Habib, S.; Ayaz, Q.; Mustafa, S.; Amin, T.; Malik, A.R.; Hussain, S.Z. Optimizing Prodigiosin Nanoencapsulation in Different Wall Materials by Freeze Drying: Characterization and Release Kinetics. Food Chem. 2025, 477, 143587, doi:10.1016/j.foodchem.2025.143587.
21. Zhao, K.; Li, D.; Cheng, G.; Zhang, B.; Han, J.; Chen, J.; Wang, B.; Li, M.; Xiao, T.; Zhang, J.; et al. Targeted Delivery Prodigiosin to Choriocarcinoma by Peptide-Guided Dendrigraft Poly-l-Lysines Nanoparticles. Int. J. Mol. Sci. 2019, 20, 5458, doi:10.3390/ijms20215458.
22. Rastegari, B.; Karbalaei-Heidari, H.R.; Zeinali, S.; Sheardown, H. The Enzyme-Sensitive Release of Prodigiosin Grafted β-Cyclodextrin and Chitosan Magnetic Nanoparticles as an Anticancer Drug Delivery System: Synthesis, Characterization and Cytotoxicity Studies. Colloids Surfaces B Biointerfaces 2017, 158, 589–601, doi:10.1016/j.colsurfb.2017.07.044.
23. Darya, G.H.; Zare, O.; Karbalaei-Heidari, H.R.; Zeinali, S.; Sheardown, H.; Rastegari, B. Enzyme-Responsive Mannose-Grafted Magnetic Nanoparticles for Breast and Liver Cancer Therapy and Tumor-Associated Macrophage Immunomodulation. Expert Opin. Drug Deliv. 2024, 21, 663–677, doi:10.1080/17425247.2024.2347300.
24. Dozie-Nwachukwu, S.O.; Danyuo, Y.; Obayemi, J.D.; Odusanya, O.S.; Malatesta, K.; Soboyejo, W.O. Extraction and Encapsulation of Prodigiosin in Chitosan Microspheres for Targeted Drug Delivery. Mater. Sci. Eng. C 2017, 71, 268–278, doi:10.1016/j.msec.2016.09.078.
25. Nwazojie, C.C.; Obayemi, J.D.; Salifu, A.A.; Borbor-Sawyer, S.M.; Uzonwanne, V.O.; Onyekanne, C.E.; Akpan, U.M.; Onwudiwe, K.C.; Oparah, J.C.; Odusanya, O.S.; et al. Targeted Drug-Loaded PLGA-PCL Microspheres for Specific and Localized Treatment of Triple Negative Breast Cancer. J. Mater. Sci. Mater. Med. 2023, 34, 41, doi:10.1007/s10856-023-06738-y.
26. Conde-Vancells, J.; Rodriguez-Suarez, E.; Embade, N.; Gil, D.; Matthiesen, R.; Valle, M.; Elortza, F.; Lu, S.C.; Mato, J.M.; Falcon-Perez, J.M. Characterization and Comprehensive Proteome Profiling of Exosomes Secreted by Hepatocytes. J. Proteome Res. 2008, 7, 5157–5166, doi:10.1021/pr8004887.
27. Sharma, S.; Masud, M.K.; Kaneti, Y.V.; Rewatkar, P.; Koradia, A.; Hossain, M.S.A.; Yamauchi, Y.; Popat, A.; Salomon, C. Extracellular Vesicle Nanoarchitectonics for Novel Drug Delivery Applications. Small 2021, 17, doi:10.1002/smll.202102220.
28. Kumar, M.A.; Baba, S.K.; Sadida, H.Q.; Marzooqi, S.A.; Jerobin, J.; Altemani, F.H.; Algehainy, N.; Alanazi, M.A.; Abou-Samra, A.-B.; Kumar, R.; et al. Extracellular Vesicles as Tools and Targets in Therapy for Diseases. Signal Transduct. Target. Ther. 2024, 9, 27, doi:10.1038/s41392-024-01735-1.
29. Kodam, S.P.; Ullah, M. Diagnostic and Therapeutic Potential of Extracellular Vesicles. Technol. Cancer Res. Treat. 2021, 20, doi:10.1177/15330338211041203.
30. Arendt, B.K.; Walters, D.K.; Wu, X.; Tschumper, R.C.; Jelinek, D.F. Multiple Myeloma Cell-Derived Microvesicles Are Enriched in CD147 Expression and Enhance Tumor Cell Proliferation. Oncotarget 2014, 5, 5686–5699, doi:10.18632/oncotarget.2159.
31. Menck, K.; Sivaloganathan, S.; Bleckmann, A.; Binder, C. Microvesicles in Cancer: Small Size, Large Potential. Int. J. Mol. Sci. 2020, 21, 5373, doi:10.3390/ijms21155373.
32. Shan, C.; Liang, Y.; Wang, K.; Li, P. Mesenchymal Stem Cell-Derived Extracellular Vesicles in Cancer Therapy Resistance: From Biology to Clinical Opportunity. Int. J. Biol. Sci. 2024, 20, 347–366, doi:10.7150/ijbs.88500.
33. Zhou, M.; Li, H.; Zhao, J.; Zhang, Q.; Han, Z.; Han, Z.-C.; Zhu, L.; Wang, H.; Li, Z. Extracellular Vesicles Derived from Mesenchymal Stem Cells Suppress Breast Cancer Progression by Inhibiting Angiogenesis. Mol. Med. Rep. 2024, 30, 192, doi:10.3892/mmr.2024.13316.
34. Luo, T.; von der Ohe, J.; Hass, R. MSC-Derived Extracellular Vesicles in Tumors and Therapy. Cancers (Basel). 2021, 13, 5212, doi:10.3390/cancers13205212.

 doi:10.20944/preprints202512.1280.v1

35. Vafaeizadeh, M.; Abroun, S.; Soufi Zomorrod, M. Effect of Human Bone Marrow Mesenchymal Stem Cell-Derived Microvesicles on the Apoptosis of the Multiple Myeloma Cell Line U266. J. Cancer Res. Clin. Oncol. 2024, 150, 299, doi:10.1007/s00432-024-05822-2.
36. Lee, B.-C.; Kang, I.; Yu, K.-R. Therapeutic Features and Updated Clinical Trials of Mesenchymal Stem Cell (MSC)-Derived Exosomes. J. Clin. Med. 2021, 10, 711, doi:10.3390/jcm10040711.
37. Yagi, H.; Soto-Gutierrez, A.; Parekkadan, B.; Kitagawa, Y.; Tompkins, R.G.; Kobayashi, N.; Yarmush, M.L. Mesenchymal Stem Cells: Mechanisms of Immunomodulation and Homing. Cell Transplant. 2010, 19, 667–679, doi:10.3727/096368910X508762.
38. Li, S.; Zhang, J.; Sun, L.; Yang, Z.; Liu, X.; Liu, J.; Liu, X. Mesenchymal Stem Cell-Derived Extracellular Vesicles: Current Advances in Preparation and Therapeutic Applications for Neurological Disorders. Front. Cell Dev. Biol. 2025, 13, doi:10.3389/fcell.2025.1626996.
39. Roszkowski, S. Therapeutic Potential of Mesenchymal Stem Cell-Derived Exosomes for Regenerative Medicine Applications. Clin. Exp. Med. 2024, 24, 46, doi:10.1007/s10238-023-01282-z.
40. Zakirova, E.Y.; Valeeva, A.N.; Masgutov, R.F.; Naumenko, E.A.; Rizvanov, A.A. Application of Allogenic Adipose-Derived Multipotent Mesenchymal Stromal Cells from Cat for Tibial Bone Pseudoarthrosis Therapy (Case Report). Bionanoscience 2017, 7, 207–211, doi:10.1007/s12668-016-0306-x.
41. Chulpanova, D.S.; Gilazieva, Z.E.; Kletukhina, S.K.; Aimaletdinov, A.M.; Garanina, E.E.; James, V.; Rizvanov, A.A.; Solovyeva, V. V. Cytochalasin B-Induced Membrane Vesicles from Human Mesenchymal Stem Cells Overexpressing IL2 Are Able to Stimulate CD8+ T-Killers to Kill Human Triple Negative Breast Cancer Cells. Biology (Basel). 2021, 10, 141, doi:10.3390/biology10020141.
42. Salarpour, S.; Forootanfar, H.; Pournamdari, M.; Ahmadi-Zeidabadi, M.; Esmaeeli, M.; Pardakhty, A. Paclitaxel Incorporated Exosomes Derived from Glioblastoma Cells: Comparative Study of Two Loading Techniques. DARU J. Pharm. Sci. 2019, 27, 533–539, doi:10.1007/s40199-019-00280-5.
43. Zmievskaya, E.A.; Mukhametshin, S.A.; Ganeeva, I.A.; Gilyazova, E.M.; Siraeva, E.T.; Kutyreva, M.P.; Khannanov, A.A.; Yuan, Y.; Bulatov, E.R. Artificial Extracellular Vesicles Generated from T Cells Using Different Induction Techniques. Biomedicines 2024, 12, 919, doi:10.3390/biomedicines12040919.
44. Kutyreva, M.P.; Vagapova, A.I.; Maksimov, A.F.; Khannanov, A.A.; Ignatyeva, K.A.; Kiiamov, A.G.; Cherosov, M.A.; Emelianov, D.A.; Kutyrev, G.A. Hybrid Nanostructures of Hyperbranched Polyester Loaded with Gd(III) and Dy(III) Ions. ACS Appl. Polym. Mater. 2024, 6, 1662–1673, doi:10.1021/acsapm.3c02428.
45. Malloy, A.; Hole, P.; Carr, B. NanoParticle Tracking Analysis; The Halo System. MRS Proc. 2006, 952, 0952-F02-04, doi:10.1557/PROC-0952-F02-04.
46. Malloy, A.; Carr, B. NanoParticle Tracking Analysis – The HaloTM System. Part. Part. Syst. Charact. 2006, 23, 197–204, doi:10.1002/ppsc.200601031.
47. Midekessa, G.; Godakumara, K.; Ord, J.; Viil, J.; Lättekivi, F.; Dissanayake, K.; Kopanchuk, S.; Rinken, A.; Andronowska, A.; Bhattacharjee, S.; et al. Zeta Potential of Extracellular Vesicles: Toward Understanding the Attributes That Determine Colloidal Stability. ACS Omega 2020, 5, 16701–16710, doi:10.1021/acsomega.0c01582.
48. Karmacharya, M.; Kumar, S.; Cho, Y.-K. Tuning the Extracellular Vesicles Membrane through Fusion for Biomedical Applications. J. Funct. Biomater. 2023, 14, 117, doi:10.3390/jfb14020117.
49. Dubuke, M.L.; Munson, M. The Secret Life of Tethers: The Role of Tethering Factors in SNARE Complex Regulation. Front. Cell Dev. Biol. 2016, 4, doi:10.3389/fcell.2016.00042.
50. Dumontet, C.; Reichert, J.M.; Senter, P.D.; Lambert, J.M.; Beck, A. Antibody–Drug Conjugates Come of Age in Oncology. Nat. Rev. Drug Discov. 2023, 22, 641–661, doi:10.1038/s41573-023-00709-2.
51. Zeng, H.; Guo, S.; Ren, X.; Wu, Z.; Liu, S.; Yao, X. Current Strategies for Exosome Cargo Loading and Targeting Delivery. Cells 2023, 12, 1416, doi:10.3390/cells12101416.
52. Kim, M.S.; Haney, M.J.; Zhao, Y.; Mahajan, V.; Deygen, I.; Klyachko, N.L.; Inskoe, E.; Piroyan, A.; Sokolsky, M.; Okolie, O.; et al. Development of Exosome-Encapsulated Paclitaxel to Overcome MDR in Cancer Cells. Nanomedicine Nanotechnology, Biol. Med. 2016, 12, 655–664, doi:10.1016/j.nano.2015.10.012.

 doi:10.20944/preprints202512.1280.v1

53. Haney, M.J.; Klyachko, N.L.; Zhao, Y.; Gupta, R.; Plotnikova, E.G.; He, Z.; Patel, T.; Piroyan, A.; Sokolsky, M.; Kabanov, A. V.; et al. Exosomes as Drug Delivery Vehicles for Parkinson's Disease Therapy. J. Control. Release 2015, 207, 18–30, doi:10.1016/j.jconrel.2015.03.033.
54. Hartjes, T.A.; Mytnyk, S.; Jenster, G.W.; van Steijn, V.; van Royen, M.E. Extracellular Vesicle Quantification and Characterization: Common Methods and Emerging Approaches. Bioeng. (Basel, Switzerland) 2019, 6, 7, doi:10.3390/bioengineering6010007.
55. Zabeo, D.; Cvjetkovic, A.; Lässer, C.; Schorb, M.; Lötvall, J.; Höög, J.L. Exosomes Purified from a Single Cell Type Have Diverse Morphology. J. Extracell. Vesicles 2017, 6, doi:10.1080/20013078.2017.1329476.
56. Parisse, P.; Rago, I.; Ulloa Severino, L.; Perissinotto, F.; Ambrosetti, E.; Paoletti, P.; Ricci, M.; Beltrami, A.P.; Cesselli, D.; Casalis, L. Atomic Force Microscopy Analysis of Extracellular Vesicles. Eur. Biophys. J. 2017, 46, 813–820, doi:10.1007/s00249-017-1252-4.
57. van der Vlist, E.J.; Nolte-'t Hoen, E.N.M.; Stoorvogel, W.; Arkesteijn, G.J.A.; Wauben, M.H.M. Fluorescent Labeling of Nano-Sized Vesicles Released by Cells and Subsequent Quantitative and Qualitative Analysis by High-Resolution Flow Cytometry. Nat. Protoc. 2012, 7, 1311–1326, doi:10.1038/nprot.2012.065.
58. Soo, C.Y.; Song, Y.; Zheng, Y.; Campbell, E.C.; Riches, A.C.; Gunn-Moore, F.; Powis, S.J. Nanoparticle Tracking Analysis Monitors Microvesicle and Exosome Secretion from Immune Cells. Immunology 2012, 136, 192–197, doi:10.1111/j.1365-2567.2012.03569.x.
59. Sokolova, V.; Ludwig, A.-K.; Hornung, S.; Rotan, O.; Horn, P.A.; Epple, M.; Giebel, B. Characterisation of Exosomes Derived from Human Cells by Nanoparticle Tracking Analysis and Scanning Electron Microscopy. Colloids Surf. B. Biointerfaces 2011, 87, 146–150, doi:10.1016/j.colsurfb.2011.05.013.
60. Gardiner, C.; Di Vizio, D.; Sahoo, S.; Théry, C.; Witwer, K.W.; Wauben, M.; Hill, A.F. Techniques Used for the Isolation and Characterization of Extracellular Vesicles: Results of a Worldwide Survey. J. Extracell. vesicles 2016, 5, 32945, doi:10.3402/jev.v5.32945.
61. Théry, C.; Witwer, K.W.; Aikawa, E.; Alcaraz, M.J.; Anderson, J.D.; Andriantsitohaina, R.; Antoniou, A.; Arab, T.; Archer, F.; Atkin-Smith, G.K.; et al. Minimal Information for Studies of Extracellular Vesicles 2018 (MISEV2018): A Position Statement of the International Society for Extracellular Vesicles and Update of the MISEV2014 Guidelines. J. Extracell. Vesicles 2018, 7, 1535750, doi:10.1080/20013078.2018.1535750.
62. Diaz-Armas, G.G.; Cervantes-Gonzalez, A.P.; Martinez-Duarte, R.; Perez-Gonzalez, V.H. Electrically Driven Microfluidic Platforms for Exosome Manipulation and Characterization. Electrophoresis 2022, 43, 327–339, doi:10.1002/elps.202100202.
63. Hassanpour Tamrin, S.; Sanati Nezhad, A.; Sen, A. Label-Free Isolation of Exosomes Using Microfluidic Technologies. ACS Nano 2021, 15, 17047–17079, doi:10.1021/acsnano.1c03469.
64. Kira, A.; Tatsutomi, I.; Saito, K.; Murata, M.; Hattori, I.; Kajita, H.; Muraki, N.; Oda, Y.; Satoh, S.; Tsukamoto, Y.; et al. Apoptotic Extracellular Vesicle Formation via Local Phosphatidylserine Exposure Drives Efficient Cell Extrusion. Dev. Cell 2023, 58, 1282-1298.e7, doi:10.1016/j.devcel.2023.05.008.
65. Samwang, T.; Watanabe, N.M.; Okamoto, Y.; Umakoshi, H. Exploring the Influence of Morphology on Bipolaron–Polaron Ratios and Conductivity in Polypyrrole in the Presence of Surfactants. Molecules 2024, 29, 1197, doi:10.3390/molecules29061197.
66. Clogston, J.D.; Patri, A.K. Zeta Potential Measurement. In; 2011; pp. 63–70.